nature protocols

PROTOCOL

https://doi.org/10.1038/s41596-020-0328-2

Check for updates

In vivo compression and imaging in mouse brain to measure the effects of solid stress

Hadi T. Nia[1,2,5], Meenal Datta[1,5], Giorgio Seano[1,3,5], Sue Zhang[2], William W. Ho[1,4], Sylvie Roberge[1], Peigen Huang[1], Lance L. Munn[1] and Rakesh K. Jain[1]✉

We recently developed an in vivo compression device that simulates the solid mechanical forces exerted by a growing tumor on the surrounding brain tissue and delineates the physical versus biological effects of a tumor. This device, to our knowledge the first of its kind, can recapitulate the compressive forces on the cerebellar cortex from primary (e.g., glioblastoma) and metastatic (e.g., breast cancer) tumors, as well as on the cerebellum from tumors such as medulloblastoma and ependymoma. We adapted standard transparent cranial windows normally used for intravital imaging studies in mice to include a turnable screw for controlled compression (acute or chronic) and decompression of the cerebral cortex. The device enables longitudinal imaging of the compressed brain tissue over several weeks or months as the screw is progressively extended against the brain tissue to recapitulate tumor growth–induced solid stress. The cranial window can be simply installed on the mouse skull according to previously established methods, and the screw mechanism can be readily manufactured in-house. The total time for construction and implantation of the in vivo compressive cranial window is <1 h (per mouse). This technique can also be used to study a variety of other diseases or disorders that present with abnormal solid masses in the brain, including cysts and benign growths.

Introduction

Mechanical phenomena have tremendous influence on multiscale and multiphasic biological systems. The study of aberrant mechanics can help reveal how these forces (e.g., resulting from changes in material properties and cellular behaviors) can give rise to abnormal pathophysiology. Indeed, in oncology, atypical tissue mechanics are increasingly being recognized as a pathological hallmark of solid tumors and can drive tumorigenesis, metastasis, and treatment resistance[1,2]. We discovered that, in addition to well-known mechanical abnormalities such as increased stiffness and interstitial fluid pressure, tumors generate 'solid stress'—a mechanical force originating from and transmitted by the solid elements of the tumor, including cells and extracellular matrix[3–5]. Solid stress has been shown to promote tumor progression and hinder the delivery and efficacy of anti-cancer therapies by compressing blood and lymphatic vessels and contributing to intratumoral hypoxia[6–8].

Current experimental model systems for studying causal effects of solid stress include in vitro systems, such as cells compressed by weights[9] and tumor spheroids confined in hydrogels[3,10] or exposed to osmotic pressure[11,12], and in vivo systems using magnetic nanoparticles to impose physical force on tissues[13]. Similar tools that recapitulate extratumoral physical forces would enable mechanistic studies of the effects of solid stress on the surrounding tissue—which we have found to be largely responsible for the functional decline of the host organ[14]. We recently developed three new techniques to precisely measure solid stress in human and murine tumors: ex vivo 2D mapping (planar-cut method), sensitive estimation in small tumors/metastases ex vivo (slicing method), and in situ quantification (needle-biopsy method)[5,15].

Here, we describe a protocol for fabricating and implementing a compressive cranial window (cCW) approach for mechanistic studies of solid mechanical forces in the brain coupled with intravital imaging techniques. The transparent window enables real-time visualization of brain tissue components (e.g., neurons and blood vessels) that may be adversely affected by solid stress, which can be applied acutely or chronically (for up to weeks or months) in a controlled manner. Behavioral tests

[1]Edwin L. Steele Laboratories, Department of Radiation Oncology, Massachusetts General Hospital, Harvard Medical School, Boston, MA, USA. [2]Department of Biomedical Engineering, Boston University, Boston, MA, USA. [3]Tumor Microenvironment Laboratory, Institut Curie Research Center, Paris-Saclay University, PSL Research University, Inserm U1021, CNRS UMR3347, Orsay, France. [4]Department of Chemical Engineering, Massachusetts Institute of Technology, Cambridge, MA, USA. [5]These authors contributed equally: Hadi T. Nia, Meenal Datta, Giorgio Seano. ✉e-mail: jain@steele.mgh.harvard.edu

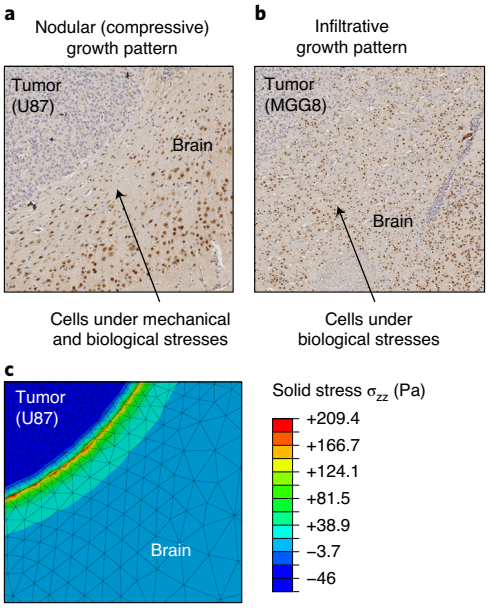

Fig. 1 | Tumor progression and brain loss are consequences of both physical and biological interactions at the tumor–brain interface. a, Tumors with nodular growth pattern (including a subpopulation of glioblastoma and most brain metastases) exert both mechanical and biological stresses on the surrounding brain tissue. **b**, Tumors with infiltrative growth pattern (i.e., the majority of glioblastomas) compress the surrounding brain less than their nodular counterparts. Scale bar, 100 μm. **c**, The solid stresses (out-of-plane component σ_{zz}) in the brain induced by a nodular tumor as quantified by the planar-cut method in conjunction with finite element modeling. **c** adapted from ref. [14], Springer Nature.

can be used without interference from the cCW, and histological and molecular evaluation of compressed brain tissues can be carried out subsequently using standardized techniques. This protocol is designed for laboratories with well-established preclinical brain disease models and expertise with intravital imaging equipment. The main requirement for successfully implementing this protocol is expertise in small-animal surgery, which is needed for cCW implantation.

Development of the protocol

Clinicians have long observed the effects of abnormal mechanical forces—edema and fluid pressure in particular—in brain tumors and the surrounding normal brain tissue. However, it was not previously possible to differentiate between the direct effects of mechanical forces resulting from solid components of the tumor tissue and the biological and physiological adverse effects exerted by the cancer cells. Although initial studies focused largely on the intratumoral effects of solid stress, we first demonstrated that there can also be substantial extratumoral forces exerted on the surrounding host organ, for example, the brain (Fig. 1; ref. [5]). We found that tumors with a nodular growth pattern (including a subpopulation of glioblastoma and most brain metastases) exert both mechanical and biological stresses on the surrounding brain tissue, whereas tumors with an infiltrative growth pattern (i.e., the majority of glioblastomas) compress the surrounding brain less than their nodular counterparts. The extratumoral forces compress the blood vessels and cells in the normal tissue surrounding the tumor[14]. Vascular collapse in the surrounding tissue can adversely impact the health of any tumor-bearing organ, but this is especially devastating in the brain. Compared with extracranial organs, the brain is unique because of its physical confinement by the skull, which can amplify mechanical force effects. Indeed, patients suffering from a primary or metastatic brain tumor are often diagnosed on the basis of an initial presentation of neurological symptoms, because the physical forces exerted by the tumor on the surrounding brain tissue directly impact physiological function[16–19]. Clinically, brain tumor mechanics are described most commonly as edema (fluid pressure) and the so-called 'mass effect' (solid stress)[20]. Although the effects of fluid pressure on brain function have been well described[21–23], we have only recently begun to explore the origins and consequences of solid stress mechanistically[14].

While examining the surrounding brain tissue in both clinical patient data and preclinical orthotopic mouse models of glioblastoma and metastatic breast cancer, we found evidence of

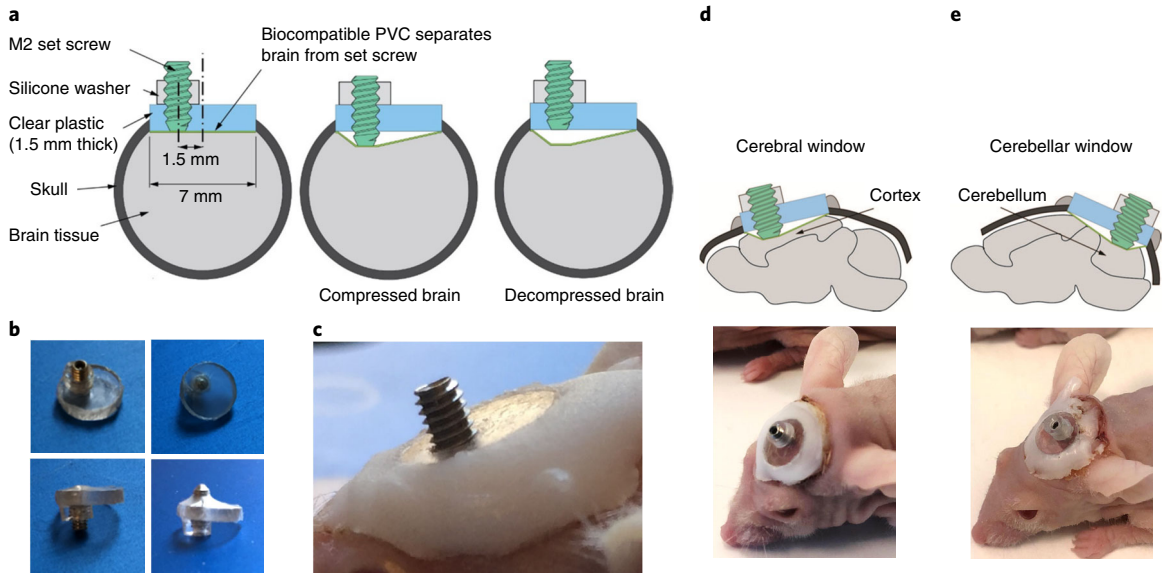

Fig. 2 | The in vivo compressive cranial window is capable of decoupling mechanical stresses from biological stresses at the tumor–brain interface. **a**, The model system comprises a set screw mounted on a transparent cranial window (left) to simulate the chronic application of compressive stress to the normal brain (center). The model also recapitulates mechanical stress relaxation after tumor removal by unloading the compression from the set screw (decompressing; right). **b**, Images of a cCW with biocompatible PVC and silicone washer from different angles in the compressed (bottom right) and uncompressed (bottom left) states. **c**, Image of the implanted compression window. **d**, cCW implanted as a cerebral window to apply chronic compression to cortex (top, schematic showing location for placement; bottom mouse with implant). **e**, cCW implanted as cerebellar window to apply chronic compression to cerebellum (top, schematic showing location for placement; bottom mouse with implant). Animal procedures in this work were carried out according to the Public Health Service Policy on Humane Care of Laboratory Animals and approved by the Institutional Animal Care and Use Committee of Massachusetts General Hospital. **a**–**c** adapted from ref. [14], Springer Nature.

profound neuronal and vascular impairment[14]. However, our standard mechanistic and intravital techniques were unable to determine whether these effects were due to only the biological effects of the cancer cells on healthy brain cells (e.g., excitotoxicity via glutamate[24–26]) or also in part to extratumoral mechanical forces. Thus, we sought to develop a methodology for applying controlled quasi-static mechanical forces to the brain to simulate the forces generated by a growing tumor. This would allow for decoupling of the physical effects of tumor growth on the surrounding brain tissue from the direct biological and biochemical interactions with the cancer cells. We adapted the well-established transparent cranial window model, which allows for longitudinal intravital imaging studies, by incorporating a set screw that could be lowered at a desired rate for acute or chronic compression of the underlying brain tissue[14] (Fig. 2). We demonstrated that neurons undergo similar morphological deformation when compressed with our device or by a growing tumor (Fig. 3). This model system is also useful in recapitulating and observing the dynamic effects of surgical removal of tumors, part of the standard of care whenever possible. The brain tissue undergoes stress relaxation and substantial deformation after removal of the tumor; this is due to release of the mechanical compression that the brain tissue experienced from the mass. Using the cCW in combination with intravital, functional, histological, and molecular assays, we demonstrated how removal of compression and subsequent brain tissue relaxation affect the neuronal, vascular, and functional activities of the surrounding normal brain[14].

Applications

In our initial studies, we demonstrated, for the first time to our knowledge, that solid stress is causally linked to vascular and neurological dysfunction in the brain, by applying and then removing chronic cerebral compression to mimic the mechanics of tumor growth and surgical resection. Furthermore, we were able to use this cCW to screen for effective therapeutic interventions capable of reducing solid stress–induced neuronal death and improving neurological function, assessed via motor coordination and neuronal survival in mice. Thus, we were able to identify lithium as an efficient agent that can protect against solid stress effects; this may enhance treatment efficacy when used in combination with anti-cancer agents for brain tumor patients in future clinical trials[14].

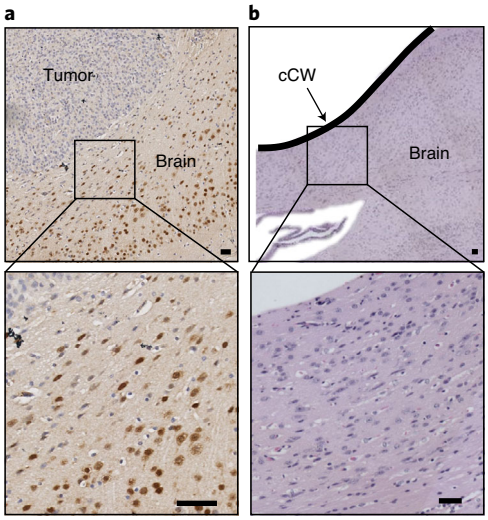

Fig. 3 | Compressive cranial window recapitulates the compressed brain tissue caused by brain tumors. a, The brain surrounding the nodular tumor is compressed, as evident by the deformed nuclei of neurons (NeuN stain). **b**, Morphologically similar compression of the neurons can be observed when the brain is compressed via cCW. Scale bars, 50 μm. Adapted from ref. [14], Springer Nature.

Beyond the study of malignant primary and secondary brain tumors, this modified cCW could be utilized in preclinical models of other diseases that present with solid masses in the brain, such as: (i) 'tumor-like' infectious lesions (including cysts or abscesses); (ii) benign masses (e.g., those resulting from abnormal neurogenesis, neurofibromatosis types I and II, tuberous sclerosis, and von Hippel–Lindau syndrome); (iii) tumefactive multiple sclerosis (MS) plaques; and (iv) extreme vascular malformations[27,28]. The modified cCW could also elucidate the role of mechanics in the progression of other brain diseases[22] and reveal novel targets for treatment. In theory, acute traumatic brain injury could also be modeled with slight modification of the cCW (i.e., by replacing the screw with a pin that freely slides in the hole, allowing high-speed, reversible compression to be applied).

The cCW can be used with mice of either sex from any genetic background; for example, we have used it successfully with both nude[14] and C57BL/6 (data not shown) male and female mice. However, the protocol is optimized for adult mice, as the skulls of juvenile mice are still growing, which compromises cCW implantation and healing (see 'Advantages and limitations'). The methods described here for cCW implantation over the forebrain can be adapted to studies of the hindbrain (e.g., for models of medulloblastoma) using established cerebellar window techniques[29,30]. Finally, as demonstrated in our early findings[14], the cCW model can be used as a drug-screening platform for agents that can protect against the adverse effects of mechanical forces in the brain.

Alternative approaches

In vitro assays, such as cell culture models, have been extensively used to study the causal role of compressive[31], tensile, and shear stresses[32,33] on neuronal activity and damage. These in vitro systems enable controlled application of mechanical stress and longitudinal high-resolution imaging, although they lack the cellular diversity and interactions in the brain and the 3D architecture of the microenvironment, which play important roles in transmission of mechanical stress. These models have been improved by using 3D hydrogel–based systems to mimic the in vivo tissue architecture[33,34] and organotypic culture systems[35,36] to mimic cellular diversity and cell–cell interactions. However, they still suffer from lack of blood perfusion (a critical element for studies that involve oxygenation or nutrient/drug delivery), inflammation, and immune response. Moreover, it is usually possible to perform only short-term experiments (i.e., on the order of days). As such, complementary in vivo models are needed to elucidate the full physical, biological, and immunological response of the brain to compressive mechanical stresses.

Previous models of brain compression in vivo have been largely based on acute expansion of an epidural balloon[37–39]. These models have been used to study ischemia, hemorrhagic stroke, traumatic

brain injury, and other conditions that may affect autoregulation of cerebral blood flow and have been used to measure intracranial pressure, arteriovenous oxygen concentrations, cerebral blood flow and oxygenation, and blood–brain barrier integrity[37–40]. Some studies have even explored the effects of controlled and isotropic epidural balloon expansion on the elastic properties of brain tissue, including compaction and stiffening of the compressed site[41–43]. A major limitation of these systems is the lack of compatibility with high-resolution intravital microscopy to monitor the consequences of mechanical compression longitudinally via optical imaging. One of the advantages of our model system is that it enables longitudinal intravital microscopy during both the compression and decompression stages. Another key advantage is the ability to precisely control the magnitude and rate of mechanical displacement.

Advantages and limitations

This protocol enables unprecedented investigation of the causal effects of tumor-generated mechanical forces on the surrounding brain tissue, coupled with dynamic intravital imaging. Laboratories that have access to these types of imaging platforms will be able to easily implement these methods (described in detail in the 'Experimental design' section). As discussed above (under 'Applications'), the device can also be easily adapted for different applications. The screw dimensions and window thickness can be readily tailored to the application or disease model of interest, and the inclusion of the biocompatible membrane that isolates the screw from the cortex ensures that the metal does not come into direct contact with brain cells and the cerebrospinal fluid does not leak.

Another key advantage is the potential to use this tool in combination with other assays and models. We have found that the cCW does not interfere with normal cage behavior[14], so behavioral tests can be performed without confounding factors. The healing process following cCW implantation is rapid, so this device can also be used in an orthotopic tumor model by implanting the cCW 10–14 d before tumor implantation.

The main potential limitation of using our device is the requirement for relatively advanced expertise in animal surgery for implantation of the cCW. We recommend housing mice bearing cCWs in isolation to prevent potential damage to the window by cage-mates, which could increase associated housing costs. If a pediatric mouse model is required (e.g., medulloblastoma), researchers may encounter issues when implanting the cCW in mice that are younger than 4 weeks of age because of continued skull growth while aging[29,30]. Thus, we recommend implanting the cCW into mice that are ≥4 weeks old. In addition, although intravital imaging can be used for the surrounding tissue, the tissue directly under the screw is obstructed.

Three main confounding factors that cannot be resolved by mechanistic use of this compression device influence biological readouts. First, the forces generated by tumor growth can be exerted in all directions, both intra- and extratumorally, whereas the cCW exerts force only in the direction in which the set screw is lowered from the surface of the brain. Although the growth-induced compressive forces that tumors exert on the surrounding brain tissue can be reasonably modeled with the cCW, the advancement of the screw also exerts shear stresses on the brain. However, we minimize the shear stress components at the interface of the cCW and the brain by incorporating a PVC membrane with a low friction coefficient to separate the device from the tissue. Second, because solid stress compresses blood vessels, the effects of mechanics versus hypoxia cannot be decoupled. For example, if neuronal damage is observed, it may be directly due to the compression or due in part to ischemic injury from compromised blood flow from compressed vessels. Third, blood vessel compression can also lead to increased interstitial fluid pressure; thus, it can be difficult to distinguish whether fluid or solid components are responsible for any downstream mechanical effects.

Experimental design

Surgery and follow-up care

This protocol, as with standard cranial window implantations, allows for a portion of the skull to be removed and coverslip to be placed in a single surgical procedure (Fig. 4). Although we have not observed substantial glial activation after window implantation in previous studies[29], we recommend waiting 10–14 d for the potential inflammatory response to surgery to subside before compression and imaging. If it is desired to implant tumor cells, this can be done in a second surgical procedure after this period. Unless required for the disease model of interest, we recommend removing the dura mater during the implantation procedure, so as not to compromise the optical quality over time. Longitudinal imaging can be performed for several months before skull regrowth occurs.

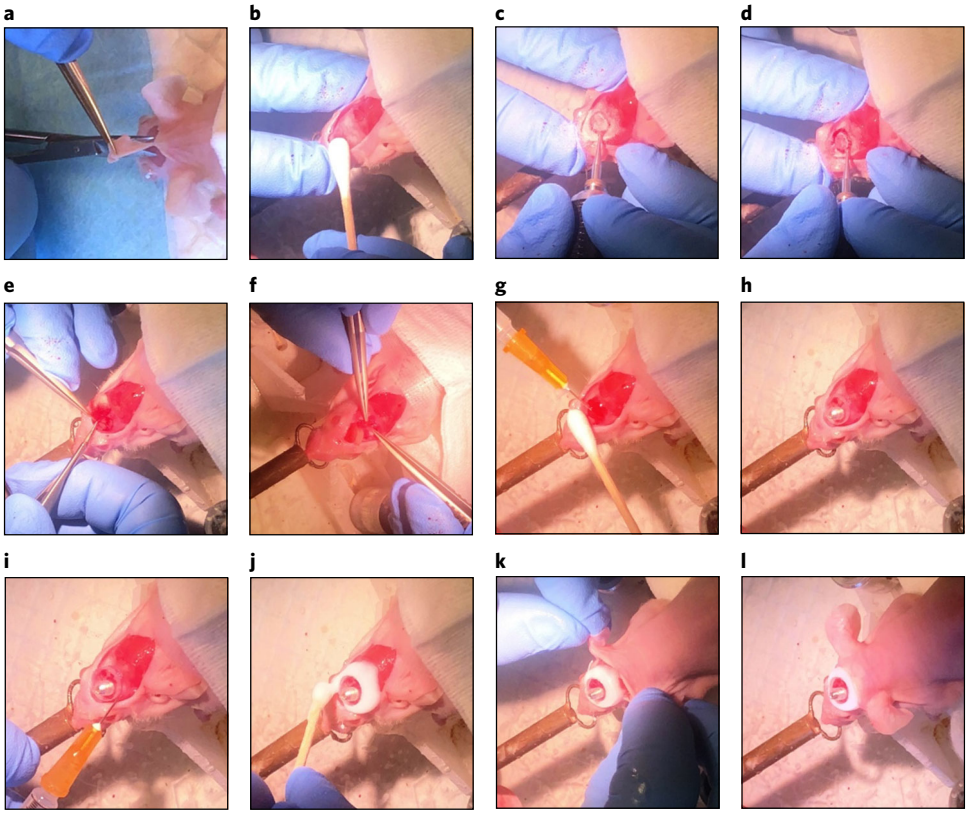

Fig. 4 | Surgical procedure for implanting a cCW. a, Skin is removed to expose the skull. **b**, The connective tissues are cleaned with a cotton swab. **c**, A circular groove is made in the skull via a handheld bone drill and fine burr tip. **d**, After washing the debris, the groove is deepened until the disk of bone is fully released. **e**, The bone and dura membrane are removed gently to avoid hemorrhage at the brain cortex. **f**, The bone residue is removed carefully to avoid regrowth. **g**, The brain is washed multiple times with saline. **h**, The cCW is placed at the desired anatomical location. **i**, Saline is injected beneath the window to stop diffusion of the glue beneath the window. **j**, Glue, premade in a Petri dish, is applied between the window and the surrounding skull bone. **k**, The skin is brought into contact with the glue. **l**, The mouse is brought back to the cage after the glue cures (<10 min). *R*, radius. Animal procedures in this work were carried out according to the Public Health Service Policy on Humane Care of Laboratory Animals and approved by the Institutional Animal Care and Use Committee of Massachusetts General Hospital.

Application of compression and decompression

The magnitude and rate of compression can be modified to recapitulate the growth of the tumor type of interest. Figure 5 shows an example loading profile that recapitulates the growth of a mouse model of glioblastoma. The displaced brain volume, V, can be estimated for general cCW dimensions from the following equation based on the conical section imposed by the PVC membrane:

$$V = \frac{\pi h}{3}\left(R_1^2 + R_1 R_2 + R_2^2\right)$$

where h is the distance the screw has traveled below the window (one full turn advances/lowers the screw by one pitch size, here 0.4 mm for an M2 screw), R_1 is the radius of the screw (here, $R_1 = 1$ mm), and R_2 is the radius of the cranial window (here, $R_2 = 3.5$ mm).

Intravital imaging modalities

The window and set screw material are chosen based on the desired imaging modality (Table 1), such as MRI, multiphoton laser-scanning microscopy (MPLSM), and optical coherence tomography (OCT) (Fig. 6). For example, MRI can be used for a variety of techniques (e.g., perfusion, tractography, elastography[44–46]). MPLSM is highly desirable for the visualization of cellular structures (including vascular ones), especially when imaging stromal components in fluorescent reporter

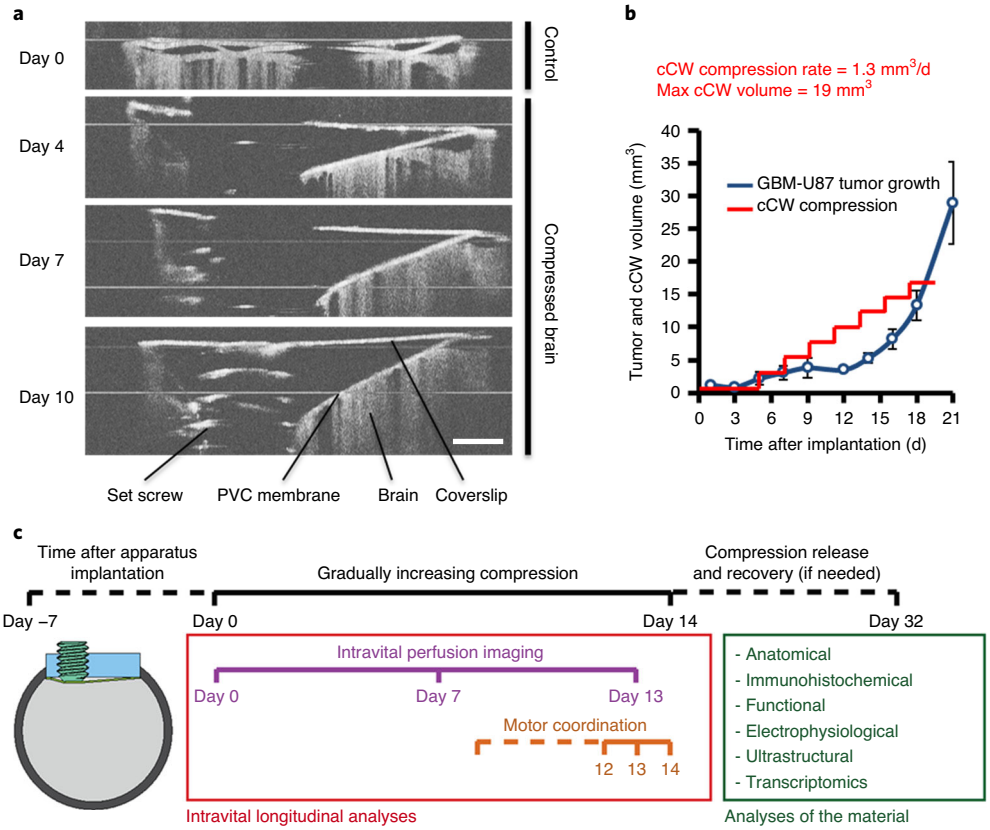

Fig. 5 | Timing and experimental design of cCW. a, The compressed brain is visualized by OCT imaging on days 0, 4, 7 and 10. Scale bar, 1 cm. **b**, A sample timing of compression associated with growth rate of a mouse model of glioblastoma (U87 cells). **c**, A sample experimental design for chronic compression of the brain and follow-up biological and physiological readouts. **c** adapted from ref. [14], Springer Nature.

Table 1 | Summary of intravital imaging techniques that can be coupled with utilization of the cCW

Imaging modality	Window material	Set screw material	Readouts
Magnetic resonance imaging (MRI)	Plastic	Plastic	Compression (set-screw) volume Tumor volume (or other disease mass) Edema/water content Blood flow/perfusion Tractography Elastography
Multiphoton laser-scanning microscopy (MPLSM)	Glass	Metal	Blood flow/perfusion Fluorescent reporters (reporter mice; labeled cells, drugs, or tracers)
Optical coherence tomography (OCT)	Glass	Metal	Compression (set screw) volume Tumor volume (or other disease mass) Blood flow/perfusion
^{18}F-FDG-PET/CT	Plastic	Plastic	Compression (set-screw) volume Tumor volume (or other disease mass) Glucose uptake

^{18}FDG-PET/CT, ^{18}fluorodeoxyglucose–positron emission tomography/computed tomography.

mouse models or via second harmonic generation, as well as when using fluorescently labeled injected cells, drugs, or tracers[47–49]. For mechanistic insight into vascular perfusion and blood flow rates, Doppler OCT offers a robust and rapid modality with resolution at the microvascular scale[50–52].

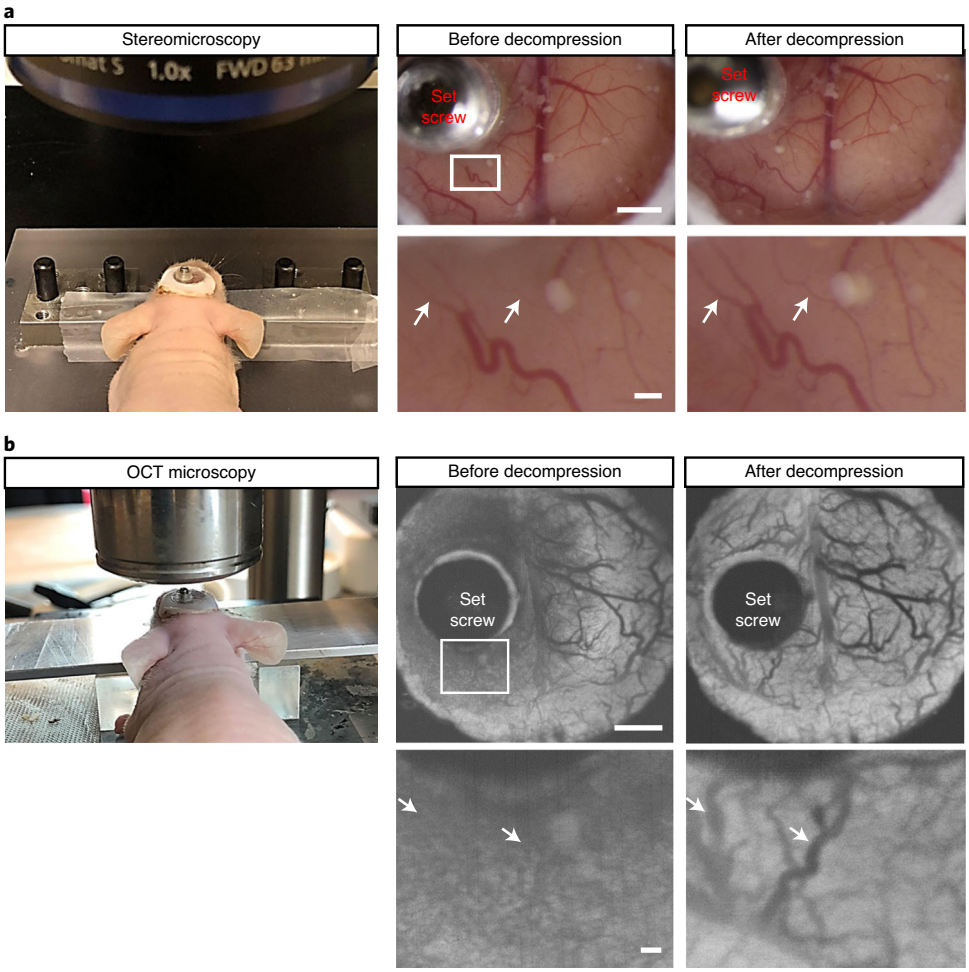

Fig. 6 | The cCW allows for intravital imaging. a,b, Setup (left) and sample images (right) via high-resolution stereomicroscopy (**a**) and optical coherence tomography (OCT; **b**) before and after decompression of the brain by reversing the set screw. White boxes represent the enlarged areas shown below the top right-hand images in **a** and **b**. Intravital microscopy allows us to follow the same anatomical structures over the time; white arrows indicate blood vessels undergoing perfusion changes before and after decompression. Scale bar, 1 cm (top images) and 100 μm (closeup magnifications). Parts of **a** and **b** adapted from ref. [14], Springer Nature. Animal procedures in this work were carried out according to the Public Health Service Policy on Humane Care of Laboratory Animals and approved by the Institutional Animal Care and Use Committee of Massachusetts General Hospital.

Solid stress measurements

We have quantified solid stress in brain tumors both intratumorally and extratumorally in the surrounding normal brain[5,14]. However, these methods have not yet been used in the tissue surrounding the set screw in mouse brains bearing the cCW. Using our recently developed techniques[5,15]—specifically, the needle-biopsy method—it is possible to measure the magnitude of solid stress (and the associated stored elastic energy) in the surrounding tissue. The required methodologies are described in detail in ref. [15].

Controls

The appropriate controls for experiments involving compression are mice that have also been implanted with the cCW but do not undergo compression/decompression using the screw.

Materials

Biological materials

- Mice. Mouse models as appropriate for clinically relevant investigations of human disease/disorders. For example, athymic nude mice can be used for allogeneic tumor growth (Nu/J; Jackson Laboratory, cat. no. 002019). **! CAUTION** All animal studies must be reviewed and approved by the relevant institutional animal care and use committees and must conform to all relevant ethics regulations. Animal procedures in this work were carried out according to the Public Health Service Policy on Humane Care of Laboratory Animals and approved by the Institutional Animal Care and Use Committee of Massachusetts General Hospital **▲ CRITICAL** For experiments meant to recapitulate pediatric disease (e.g., medulloblastoma), we recommend using 4- to 6-week-old mice so that they are still juveniles, but not so young that rapid skull growth will interfere with the cCW.

Reagents

- PBS (1×; CellGro, cat. no. 20-031-CV)
- Sterile saline, for irrigation (0.9% (wt/vol), Owens & Minor, cat. no. 0706-2F7123)
- Formaldehyde (10% (wt/vol), Polysciences, cat. no. 04018-1)

Anesthesia

- Ketamine (Ketaset, 100 mg/mL; Patterson Veterinary, cat. no. 07-803-6637)
- Xylazine (Anased, 100 mg/mL; Patterson Veterinary, cat. no. 07-808-1039)
- Sterile saline, for irrigation (0.9% (wt/vol), Owens & Minor, cat. no. 0706-2F7123)

Analgesia

- Buprenorphine (Buprenex, 0.3 mg/ml; Patterson Veterinary, cat. no. 07-850- 2280); used at a concentration of 0.1 mg/kg **▲ CRITICAL** Buprenorphine should be injected subcutaneously.
- Carprofen (Rimadyl, 50 mg/ml; Patterson Veterinary, cat. no. 07-844-7425); used at a concentration of 5 mg/kg **▲ CRITICAL** Carprofen should be injected subcutaneously.

Equipment

- Stereotactic frame (Harvard Apparatus, cat. no. 75-1808)
- Bright-field stereomicroscope (Olympus, model no. SZ61)
- Thermal pad (Shor-Line, cat. no. 712.0000.04)
- High-speed bone micro-drill, for brain surgery (Harvard Apparatus, cat. no. PY272-4950)
- Burr tip for micro-drill (Fine Science Tools, cat. no. 19007-14)
- Ophthalmic lubricant (Henry Schein, cat. no. 07-805-4502)
- (Optional) Glass coverslips (7-mm diameter, 2 mm thick; these are custom cut in-house from commercially available slides (Fisher, cat. no. 7-CIR-1-Fisher))
- (Optional) Polyethylene coverslips (7-mm diameter, 2 mm thick; these are custom cut in-house from commercially available slides (Ted Pella, cat. no. 2225))
- Stainless-steel set screws (M2 × 5 mm; McMaster-Carr, cat. no. 92605A047)
- Plastic (nylon) screw (McMaster-Carr, cat. no. 92492A703)
- Allen screwdriver for M2 set screws (McMaster-Carr, cat. no. 6958A22)
- Phillips screwdriver no. 0 for plastic screws (McMaster-Carr, cat. no. 5682A91)
- Drill bit (1/16 inch; McMaster-Carr, cat. no. 2901A111)
- M2 tap (McMaster-Carr, cat. no. 8305A77)
- Tap wrench (McMaster-Carr, cat. no. 246A23)
- Polyvinyl chloride (PVC) membrane (0.1 mm thick, 10-mm diameter; McMaster-Carr, cat. no. 8562K11)
- Silicone disk (1/16 inch thick, 3-mm diameter; McMaster-Carr, cat. no. 2183T3)
- Disposal biopsy punches (1.5-, 3-, 6-, and 10-mm diameters; Integra-Miltex, cat. nos. 33-31A, 33-32, 33-36, and 33-38)
- Syringe for anesthesia (1 mL; BD, cat. no. 309659)
- Sterile Petri dishes (various sizes, Falcon)
- Sterile gauze (Curity, cat. no. 6939)
- Sterile cotton-tip applicators (Owens & Minor, cat. no. WOD1002)
- Sterile Gelfoam (hemostat size 100; McKesson, cat. no. 189842)
- Sponges (3 inches × 3 inches; Cardinal Health, cat. no. 3307394)
- Cyanoacrylate ('super') glue (all-purpose, Krazy Glue, cat. no. KG517)
- Extra-fine acrylic powder (dental or nail grade; Keystone Industries, cat. no. 166264)

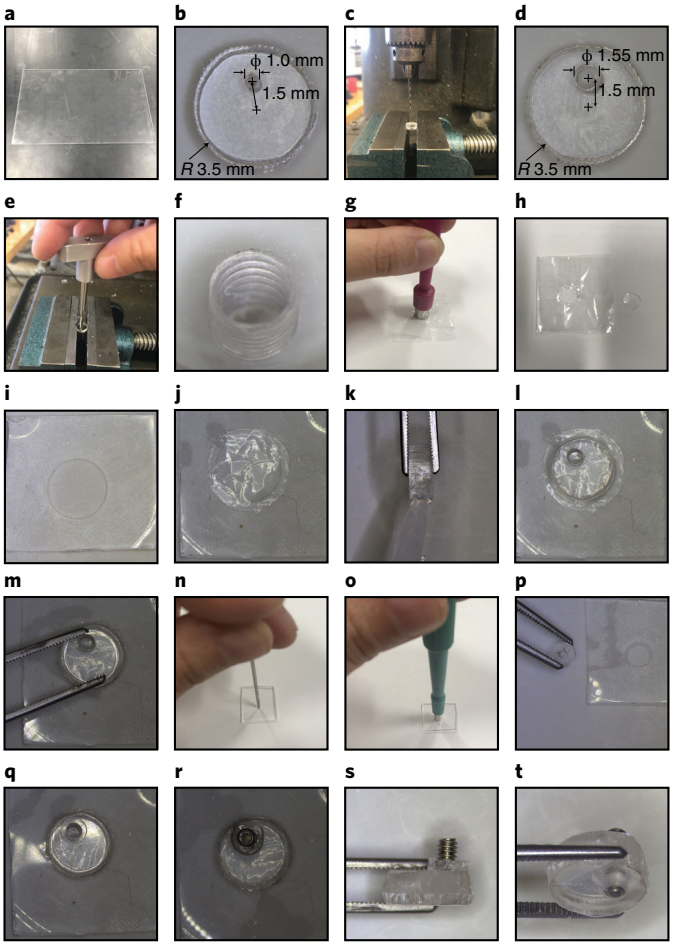

Fig. 7 | Procedure for fabrication of a cCW. a, Two-millimeter-thick polyethylene plate. **b**, Circular coverslips with 0.8-mm-diameter holes are cut from the polyethylene plate with a laser cutter. **c**, The coverslip is secured with a drill press vise. The pre-cut hole in the coverslip is aligned with the drill bit on the drill press. **d**, The hole made by the laser cutter is enlarged to 1.55 mm in diameter. **e**, Using an M2 hand tap, screw threads are created in the hole on the coverslip. **f**, Close-up of the screw threads created in the 1.55-mm diameter hole. **g**, A 10-mm disk is punched from a PVC sheet using a 10-mm biopsy punch. **h**, The 10-mm disk next to the PVC sheet. **i**, A 7-mm biopsy punch is used to create a hole in the 2-mm-thick silicone sheet. **j**, The PVC membrane is centered on top of the 7-mm hole in the silicone sheet. **k**, Cyanoacrylate ("super") glue is carefully spread along the edge of the coverslip. **l**, The coverslip with wet glue is centered on top of the PVC membrane. **m**, The coverslip is pushed onto the PVC membrane and into the hole in the silicone sheet. **n**, Make silicone washers by first punching a 1.5-mm hole in the 2-mm-thick silicone sheet. **o**, A 3-mm punch is used to cut a disk concentric with the 1.5-mm hole to create a donut-shaped silicone washer. **p**, The resulting silicone washer. **q**, Center the silicone washer with the hole in the coverslip, on the opposite the side of the PVC membrane. **r**, Screw an M2 screw into the coverslip from the side of the silicone washer until the tip of the screw touches the PVC membrane. **s**, Side-view of the finished cCW. **t**, Angled top view of the finished cCW.

- Straight iris scissors (Bonn, cat. no. RS-5840)
- Spring scissors (Vannas; Bonn, cat. no. RS-5611)
- Straight forceps (Bonn, cat. no. RS-8140)
- Dumont forceps (no. 3; Bonn, cat. no. RS-5042)
- Dumont forceps (no. 5; Bonn, cat. no. RS-5045)
- Laser cutter (Epilog Legend Series, Mini 18)
- Standard drill press
- Pen (skin marker)

Reagent setup

Ketamine–xylazine cocktail

Using aseptic technique, add 3 ml of ketamine (diluted to 10 mg/ml) and 0.3 ml of xylazine (diluted to 1 mg/ml) to 27 ml of sterile saline. This will result in a 10:1 ratio of anesthetics to saline. Store the

cocktail at room temperature (25 °C) for up to 7 d or at 4 °C for up to 30 d ▲ CRITICAL Administer the ketamine–xylazine cocktail via i.p. injection at a dose of 1 ml per 100 g body weight.

Equipment setup

cCW fabrication

Cut a coverslip from a 2-mm-thick polyethylene plate (Fig. 7a) as a 7-mm disk with a 0.5-mm-diameter hole 2 mm away from the edge, that is, 1.5 mm from the center (Fig. 7b). Use a laser cutter with settings of 20%/100%/5,000 Hz (speed/power/frequency). The tolerance of the laser cutter is ~0.3 mm at these settings. The outer diameter of the coverslip is 7 ± 0.3 mm. The diameter of the hole has a tolerance of 0.3 mm. (We recommend that users perform a few trials with their laser cutter to find specific settings that reproduce these tolerances with their equipment.) Secure the coverslip with a drill press vise and enlarge the 0.5-mm diameter-hole using a drill press with a 1.55-mm diameter drill bit (Fig. 7c,d). Set the drill speed to 500 r.p.m. Owing to the small diameter of the drill bit, heating is minimal. Use an M2 tap to create screw threads in the 1.55-mm-diameter hole in the coverslip (Fig. 7e,f).

Attach the coverslip to the PVC membrane. The PVC membrane separates the brain tissue from the screw and coverslip. Use a 10-mm punch to create a 10-mm disk out of the PVC sheet (Fig. 7g,h). Use a 7-mm punch to make a hole in a 3 cm × 3-cm, 2-mm-thick silicone sheet (Fig. 7i). Use the hole left in this silicone membrane as a template for attachment of the PVC membrane to the coverslip (Fig. 7j). Apply cyanoacrylate glue to the edge of the coverslip (without the screw attached; Fig. 7k). Make sure the glue covers the side edge but does not spread to the flat surfaces of the coverslip. Spread a thin layer of glue on a Petri dish, and roll the edge of the coverslip through the glue for a consistent and even application. Once the glue is applied to the edge of the coverslip, place a PVC membrane disk centered on top of the 7-mm hole left in the silicone sheet. Place the coverslip centered on top of the membrane (Fig. 7l). Push the coverslip so both the coverslip and the PVC membrane below it are squeezed into the 7-mm hole in the silicone sheet (Fig. 7m). In this process, the extra PVC folds on the edge of the coverslip where the glue has been applied, ensuring that equal pressure is applied to the membrane for consistent attachment.

Make silicone washers by first punching a 1.5-mm hole in the 2-mm-thick silicone sheet (Fig. 7n). Next, use the 3-mm punch to cut a disk centered on the first 1.5-mm hole (Fig. 7o). This results in a donut-shaped silicone washer (Fig. 7p). This silicone washer secures the screw in place in the coverslip with minimal recoil and prevents unintended turning. Center the silicone washer around the threaded hole in the coverslip on the face opposite the PVC membrane (Fig. 7q). Screw an M2 screw into the coverslip (Fig. 7r) until it touches the PVC membrane on the other side (Fig. 7s,t).

Procedure

Surgery ● Timing 45 min

▲ CRITICAL See Fig. 4 for images of sequential surgical steps.

1 Administer carprofen s.c. at a dose of 5 mg/kg body weight 30 min before surgery. Anesthetize the mouse with i.p. administration of 1 ml per 100 g body weight of the ketamine and xylazine cocktail. Test that the mouse is fully anesthetized via pedal reflex and respiration monitoring.
! CAUTION All experiments with mice must be performed according to institutional and national regulations and guidelines.

2 Apply ophthalmic lubricant to the eyes once the mouse is fully anesthetized.

3 Using the straight iris scissors, remove a 10-mm circular area of skin and connective tissue from the skull. Expose and clean the connective tissue and skull with a sterile cotton swab and rinse with sterile saline.
▲ CRITICAL STEP The location of this tissue removal must be made above the anatomical location of interest as dictated by the use of clinically relevant mouse models (e.g., over the forebrain or hindbrain).
▲ CRITICAL STEP Bleeding may occur due to disruption of local blood vessels. This can be controlled with Gelfoam and cotton swabs, and repeated rinsing with sterile saline.
? TROUBLESHOOTING

4 Place the mouse in the chosen stereotactic frame and position the head under the stereomicroscope.
▲ CRITICAL STEP Ensure that the mouse is stably secured and correctly positioned. The following steps (Steps 5–12) will be performed under a stereomicroscope.

5 Mark a 6-mm circle over the exposed region of interest on the skull with a pen (e.g., skin marker).

6 Equipped with a 1.4-mm-diameter burr tip, use the micro-drill to make a groove at the border of the marked circle.
▲ **CRITICAL STEP** Proceed with this drilling step slowly to avoid damage, and regularly rinse the area with cold saline to avoid thermally induced injury to the brain or surrounding skull.
? TROUBLESHOOTING

7 Over subsequent repetitive drillings, gradually increase the depth of the groove until the circular disk of bone becomes loose or the surface of the brain tissue becomes visible.
▲ **CRITICAL STEP** Be sure to avoid applying excessive pressure, which could damage the brain. Maintain constant drill motion to avoid heating damage to the brain or surrounding skull.
▲ **CRITICAL STEP** Bleeding may occur because of disruption of local blood vessels. This can be controlled with Gelfoam and cotton swabs, and repeated rinsing with sterile saline.
? TROUBLESHOOTING

8 Use the no. 3 Dumont forceps to carefully separate the circular bone disk from the dura mater underneath.
▲ **CRITICAL STEP** Proceed with this step very slowly so as not to damage the brain surface vasculature; rinse with sterile saline during bone flap removal.
▲ **CRITICAL STEP** The dura mater may tear, resulting in bleeding. This can be controlled with Gelfoam and cotton swabs, and repeated rinsing with sterile saline.
? TROUBLESHOOTING

9 Once the bone flap is removed, place a piece of Gelfoam soaked in 0.9% (wt/vol) sterile saline on the dura mater and apply sterile saline to the exposure site as necessary to keep the tissue hydrated. Using the no. 3 Dumont forceps, remove any remaining pieces of bone from the edge of the circular disk.

10 (Optional) If it is desired to remove the dura mater, move the Gelfoam to the edge of the craniectomy to absorb saline or blood during this step. Using the Dumont no. 5 forceps, create a small opening to the dura mater close to the edge of the disk. Insert the microscissors into the opening and cut the dura and the arachnoid membranes from the surface of the brain. Once they have been removed, rinse the surface of the brain with sterile saline.
▲ **CRITICAL STEP** Remove the dura slowly and carefully from the bone edge, avoiding pulling the dura or applying pressure to the brain below, while making sure to avoid damage to large blood vessels.
▲ **CRITICAL STEP** Bleeding may occur because of disruption of local blood vessels. This can be controlled with Gelfoam and cotton swabs, and repeated rinsing with sterile saline.
? TROUBLESHOOTING

11 Place the fabricated cCW over the surface of the exposed brain region, using saline to keep the tissue surface wet.
▲ **CRITICAL STEP** The surrounding bone should remain dry for the next step, in which the cCW is affixed to the skull.
▲ **CRITICAL STEP** Be sure to use cCWs fabricated with coverslips of the appropriate material for the required subsequent imaging modalities (glass or plastic).
▲ **CRITICAL STEP** Avoid placing the screw over the sagittal sinus, as chronic compression of this major blood vessel could result in death.
? TROUBLESHOOTING

12 Affix the cCW to the bone using a 1:1 mixture of histocompatible cyanoacrylate glue and fine acrylic powder, making sure to apply the mixture quickly before it sets.
▲ **CRITICAL STEP** The surrounding bone must be dry to ensure proper fixation of the cCW to the glue. Do not allow the glue to contact the brain tissue directly.
? TROUBLESHOOTING

13 After surgery, monitor the mouse on the heading pad until the anesthesia wears off. Once the mouse is awake, administer buprenorphine s.c. at a dose of 0.1 mg/kg body weight.
▲ **CRITICAL STEP** Be sure to place only one mouse per cage to reduce the chance of damage to the cCW by cage-mates.
? TROUBLESHOOTING

14 Administer carprofen s.c. at a dose of 5 mg/kg body weight for pain management over the next 1–2 d, or as needed.

Table 2 | Rotation angles/turns and their associated depths and displaced brain tissue volumes for a cCW with an M2 set screw

Rotation	Depth, *h* (mm)	Displaced brain volume, *V* (mm^3)
90°	0.1	1.75
180°	0.2	3.5
360° (1 turn)	0.4	7.0
2 turns	0.8	14.0
3 turns	1.2	21.0

Applying compression and decompression ● Timing 5 min

▲ **CRITICAL** See Fig. 5 for examples of compression profiles. See Table 2 for the amount of rotation required for a desired volume displacement, estimated on the basis of thread size.

15 Anesthetize the mouse with 1 ml per 100 g body weight of the ketamine–xylazine cocktail. Test that the mouse is fully anesthetized via pedal reflex and respiration monitoring.

16 Apply the compression by turning the screw clockwise. The compression level and frequency of compression depend on the study of interest. As an example, to simulate the chronic compression due to tumor growth[14], we increased the compression by 1.3 mm^3/d (volume of compression from the screw) for 2 weeks.

17 (Optional) Use imaging methods such as OCT to verify the compression level by locating the bottom surface of the screw with respect to the top surface of the brain cortex. In case of recoil or if the screw becomes unscrewed because of mouse movement and/or intracranial pressure, adjust the compression.

18 (Optional) To simulate tumor removal, decompress the brain cortex by unscrewing the screw. The screw should be left at the coverslip (zero) level.

Imaging ● Timing variable

▲ **CRITICAL** See Fig. 6 for images of compression via OCT imaging.

19 (Optional) Anesthetize the mouse and perform intravital imaging of brain structures during solid mechanical force application through the transparent cCW (as described under 'Experimental design'). Depending on the imaging modality (e.g., OCT), the entire brain can be imaged on the order of minutes, but longer imaging studies can be performed.

! CAUTION This optional step, as with all experiments with mice, must be performed according to institutional and national regulations and guidelines.

? TROUBLESHOOTING

(Optional) Treatment ● Timing variable

20 Treat the cCW-bearing mice as any other mice bearing standard cranial windows, but use more caution when holding the mice. The thick coverslip is more prone to detachment from the skull as compared with a standard cranial window, so the mouse should be handled with care.

? TROUBLESHOOTING

(Optional) Tissue collection ● Timing 5 min

21 If you wish to perform histological analyses on tissues collected at the end of the mechanical compression studies, perform whole-animal perfusion fixation at this point to preserve the deformed geometric and architectural features of the brain tissue under compression. The entire mouse head can be removed after intracardiac perfusion with 2% (vol/vol) formaldehyde in PBS and then fixed with 2% (vol/vol) formaldehyde in PBS for 24–72 h. Then the brains can be dissected from the head and embedded in paraffin.

! CAUTION Formaldehyde is toxic and must be handled carefully under a chemical fume hood. Alternatively, brain tissue can be collected for molecular analyses (e.g., DNA, RNA, protein) using standard collection methods. This optional step, as with all experiments with mice, must be performed according to institutional and national regulations and guidelines.

Troubleshooting

Troubleshooting advice can be found in Table 3.

Table 3 | Troubleshooting table

Step	Problem	Possible reason	Solution
3, 7, 8, 10	Bleeding from skull during surgery	Damage to blood vessels	Bleeding can be controlled with Gelfoam and cotton swabs, and rinsing with sterile saline. If bleeding persists at the cCW surface after surgery, we recommend excluding the mouse from the study if the bleeding or clotting interferes with the imaging modality
6	Poor drilling and/or excessive heating of bone and tissue	Drill bit has become dull	The drill bits will wear down eventually and should be discarded and replaced after 100 cCW implantations. Drill bits should also be sterilized with dry heat
	Drill breaches skull and penetrates underlying tissue	Excess force and/or speed during drilling	Exclude mouse from experiment; proceed with slower and less forceful drilling on remaining mice in study
10, 19	Poor imaging quality	Dura mater intact	Unless required for the disease model of interest, we recommend removing the dura mater during the surgical cCW implantation procedure, so as not to compromise optical quality over time
12	Glue directly contacts the brain	Insufficient layer of saline on tissue below cCW	Saline should be applied to the exposed surface of the brain under the cCW and to the edge of the coverslip to exclude any glue that may penetrate the exposed tissue area. Be sure to apply sufficient amounts of saline and apply the glue to the surrounding (dry) bone carefully
11, 12	cCW becomes loose or dislodged	Bone was wet during application of glue	Be sure to thoroughly dry the bone surrounding the window site before adding the glue with a cotton applicator. Then add saline carefully one drop at a time to cover the surface of the brain just to the edge of the area that the window will cover
13, 20	cCW becomes loose or dislodged	Disruption/damage of cCW by cage-mates	We highly recommend housing mice individually. Researchers should account for a 5% failure rate on the basis of cCW disruption by either mouse activity or operator error
15–20	Regrowth of skull bone over cCW site	Insufficient removal of bone during implantation surgery	If compression has not yet been initiated, the cCW can be removed, the bony regrowth removed, and a new cCW implanted. However, if mechanical force studies have begun, we recommend excluding the mouse from the study if the bone is interfering with compression or imaging
	cCW becomes loose or is lost	cCW was dislodged during mouse handling	We highly recommend that the mice be handled gently and held from areas around the shoulder rather than the neck so as not to disrupt the cCW
	Lost or loose screw	The silicone washer was not in contact with coverslip	Before implanting the cCW, the silicone washer needs to be pushed toward the coverslip to make full contact in order to avoid a loose screw

Timing

On a per-mouse basis, the following timing applies:
Steps 1–14, surgery: 45 min
Steps 15–18, applying compression (and optional decompression): 5 min
Step 19, (optional) imaging: variable
Step 20, (optional) treatment: variable
Step 21, (optional) tissue collection: 5 min

Anticipated results

One of the greatest advantages of the cCW is its ability to be coupled to intravital imaging (as described in the Introduction and summarized in Table 1). We have implemented standard stereomicroscope imaging and OCT (Fig. 6). For example, via OCT imaging of perfused vessels, we found in our previous study that compression of the cortex with cCW not only compressed the tissue immediately below the screw, but also reduced the vascular perfusion in the concentric surrounding tissue. Subsequent decompression of the cortex (simulating brain tumor resection) restored vessel perfusion[14].

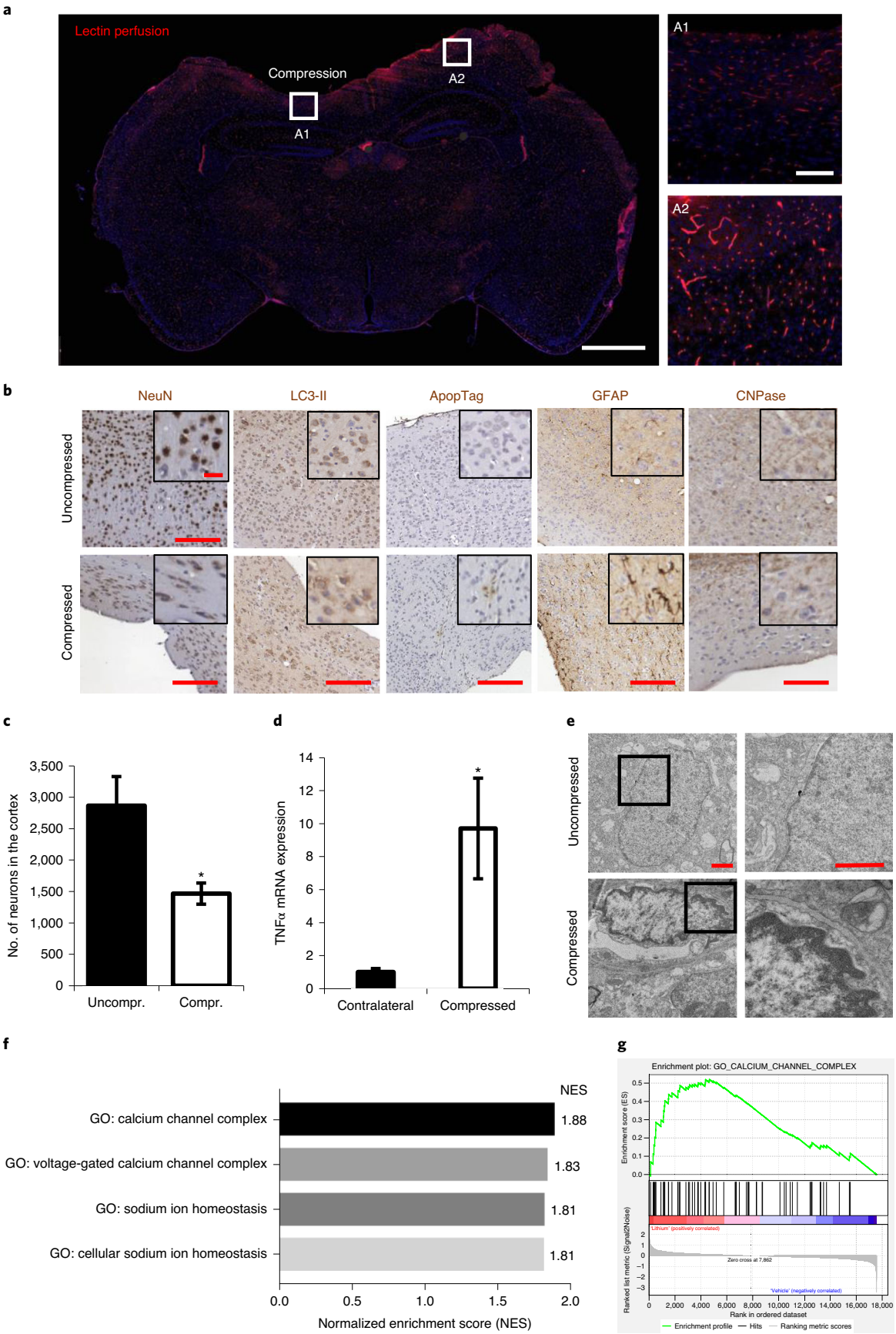
a
Lectin perfusion
Compression
A1
A2
A1
A2
b
NeuN
LC3-II
ApopTag
GFAP
CNPase
Uncompressed
Compressed
c
No. of neurons in the cortex
3,500
3,000
2,500
2,000
1,500
1,000
500
0
Uncompr.
Compr.
d
TNFα mRNA expression
14
12
10
8
6
4
2
0
Contralateral
Compressed
e
Uncompressed
Compressed
f
NES
GO: calcium channel complex
1.88
GO: voltage-gated calcium channel complex
1.83
GO: sodium ion homeostasis
1.81
GO: cellular sodium ion homeostasis
1.81
0.0
0.5
1.0
1.5
2.0
Normalized enrichment score (NES)
g
Enrichment plot: GO_CALCIUM_CHANNEL_COMPLEX
Enrichment score (ES)
Ranked list metric (Signal2Noise)
Lithium' (positively correlated)
Zero cross at 7,862
'Vehicle' (negatively correlated)
0
2,000
4,000
6,000
8,000
10,000
12,000
14,000
16,000
18,000
Rank in ordered dataset
Enrichment profile
Hits
Ranking metric scores

◀ **Fig. 8 | Chronic compression results in cellular biological responses that can be quantified via histological and molecular techniques. a**, Lectin perfusion (red) shows perfused vessels that are lowered in compressed area A1 compared with uncompressed area A2 (blue nuclear stain = DAPI). Scale bar, 1 mm. **b**, Examples of IHC staining of neuronal nuclei (NeuN), autophagy (LC3-II), apoptosis (ApopTag), activated astrocytes (GFAP), and oligodendrocytes (CNPase). Scale bars, 100 μm. **c**, Neuronal loss can be quantified from immunohistochemical (IHC) analysis. The number of neurons in the cortex was assessed by quantifying the number of $NeuN^+$ nuclei in mosaic-stitched images of the coronal sections of the region of the cortex exposed to the compression apparatus (the anterior cingulate area, the primary and secondary motor area, and the first part of the primary somatosensory area, as identified using a mouse brain atlas map[57]). *$P < .05$, Student's two-tailed unpaired t tests; $n = 4$. **d**, Gene expression of TNF-α (via qRT-PCR) increases in response to compression. *$P < .05$, Student's two-tailed unpaired t tests; $n = 3$. **e**, Chromatin condensation as a result of compression can be quantified via electron microscopy; right-hand images are close-ups of the boxes areas in the left-hand images. Scale bars, 1 μm. **f**, An example enrichment plot of gene ontology after RNA sequencing of brain tissue under chronic compression with and without treatment with lithium, a neuroprotective agent. The gene ontologies associated with calcium channel complex and sodium ion homeostasis were substantially upregulated in lithium-treated cortexes (false-discovery rate < 0.25). **g**, An example of gene set enrichment analysis (GSEA) of calcium channel complex of the brain under compressive stresses treated with lithium. The Gene Set Enrichment Analysis (GSEA) software from the Broad Institute was used to create these images. GO, gene ontology; NES, normalized enrichment score. Parts of this figure adapted from ref. [14], Springer Nature.

Table 4 | Examples of relevant markers for murine brain cell histology after acute or chronic compression with the cCW

Molecular/cellular feature	Marker
Vasculature	
Endothelial cells	CD31
Perivascular cells	Desmin, αSMA
Basement membrane	Collagen IV, laminin, agrin
Perfusion	Lectin[a], dextran[a]
Neurons	
Neural stem cells	ALDH, Nestin, SOX2
Neural progenitors	NCAM, Musashi-1
Mature neurons	NeuN, GAD
Glia	
Astrocytes	GFAP, GLAST, GLT-1
Microglia	Iba1, TMEM119
Oligodendrocytes	PDGFRα, NG2, Olig1-3, OSP
Cell proliferation/death	
Proliferation	BrdU[a], Ki-67, PCNA
Apoptosis	ApopTag, cleaved caspase-3
Autophagy	p62, Beclin-1, LC3B-II
Necroptosis	RIPK1, RIPK3, MLKL
Other microenvironmental/disease factors	
Hypoxia	Pimonidazole[a], Hif1α,
Plaques/tangles	Amyloid-β, tau
Inflammatory cytokines	IL-1β, IL-6, IL-10, TNFα

[a]Must be injected before necropsy/imaging.

Importantly, as described in Step 21, it is possible to perform histological and molecular analyses and transcriptomics on the brain tissues collected at the end of mechanical compression studies (Fig. 8). This enables characterization of brain molecular and cellular structure, as well as the effects of mechanical compression on neurological function. Table 4 summarizes potential histological markers of interest. Through histology, we have been able to compare the extent and effect of compression with the cCW with that of a brain tumor (Fig. 1), and, with the appropriate immunostaining, we have been able to study neurons, astrocytes, perfused vessels, and markers of cell death and autophagy (Fig. 8). Using quantitative image analysis, we previously showed that compression reduces neurons in the cortex and decompression partially restores a higher number of neuronal cells.

Table 5 | Potential neurological tests for mice to assess the effects of solid mechanical compression from the cCW

Test/measurement	Readout
Motor function	
Rotarod	Motor coordination, balance, ataxia
Stride length/footprint test	Balance, ataxia
Horizontal beam/string test	Forelimb strength and coordination
Elevated bridge test	Balance, ataxia
Nociception	
Hot plate/thermal probe test	Pain tolerance
Foot-shock test	Pain tolerance
Tail-pressure test	Pain tolerance
Behavior	
Open-field test	Anxiety, habituation
Acoustic test	Hearing and hippocampal function
Morris water task	Spatial learning
Dark/light avoidance	Anxiety
Maze tests	Anxiety, spatial learning, memory
Object recognition	Memory

Microanatomy can also be analyzed via electron microscopy after compression, for example, to assess condensed chromatin in apoptotic/necrotic neurons (Fig. 8d)[14].

The effects of compression (and decompression) on mechanical properties and forces in the brain can be assessed after cCW use. For example, solid stress and elastic energy can be measured using our previously established methods[5,15]. Edema can be measured ex vivo using established techniques such as wet/dry weight measurement, or in vivo via MRI[53]. Interstitial fluid pressure can be measured using the gold-standard wick-in-needle technique[54] through a hole adjacent to the set screw that is carefully drilled through the coverslip.

Mechanopathologies induced by any of the potential disease or trauma states discussed in the Introduction can promote deterioration of neurological function, motor coordination, and behavior[55]. Thus, the cCW enables direct study of the effects of compression on these functionalities in mice, which are summarized in Table 5, including Rotarod endurance and stride length (Fig. 9). We previously found that compression results in reduced Rotarod endurance and stride length in mice, whereas decompression was able to partially rescue these motor coordination deficits[14]. Compression of different regions of the cerebral and cerebellar cortex may have differential effects on neurological functions, such as motor coordination, balance, locomotion activity, memory, anxiety, and ataxia.

Another crucial application of the cCW is that of a drug-screening platform to rescue the pathological effects of abnormal solid mechanics in the brain. For example, we recently used the cCW model to screen a number of drugs known to be neuroprotective and test whether they could revert neuronal loss due to compression, and we found that lithium chloride alleviated the compression-mediated neuronal damage[14]. In addition, the transparent cranial window allows for coupling with alternative treatment techniques beyond systemic therapy, such as focused ultrasound therapy[56]. Furthermore, in addition to or instead of histology, the brain tissue can be collected for molecular dissection of DNA, RNA, and protein to assess the mechanistic effects of disease, compression/decompression, and treatment. Through bulk RNA sequencing of compressed cortical tissue, for example, we found that lithium chloride induced upregulation of genes and pathways related to neuronal differentiation and function, and downregulation of those related to cell death[14].

In conclusion, we present here the methodologies required to establish an in vivo compression apparatus that can be coupled in real time to dynamic intravital imaging modalities. Equipped with this simple, yet effective, device, scientists studying a multitude of brain diseases/conditions—from malignant tumors to traumatic brain injury—will be able to mechanistically simulate the effects of solid mechanics in their research contexts. This cCW can be used not only to understand the direct effects of such mechanics on brain cells, but also to reveal new disease treatment targets and to effectively test potential protective agents.

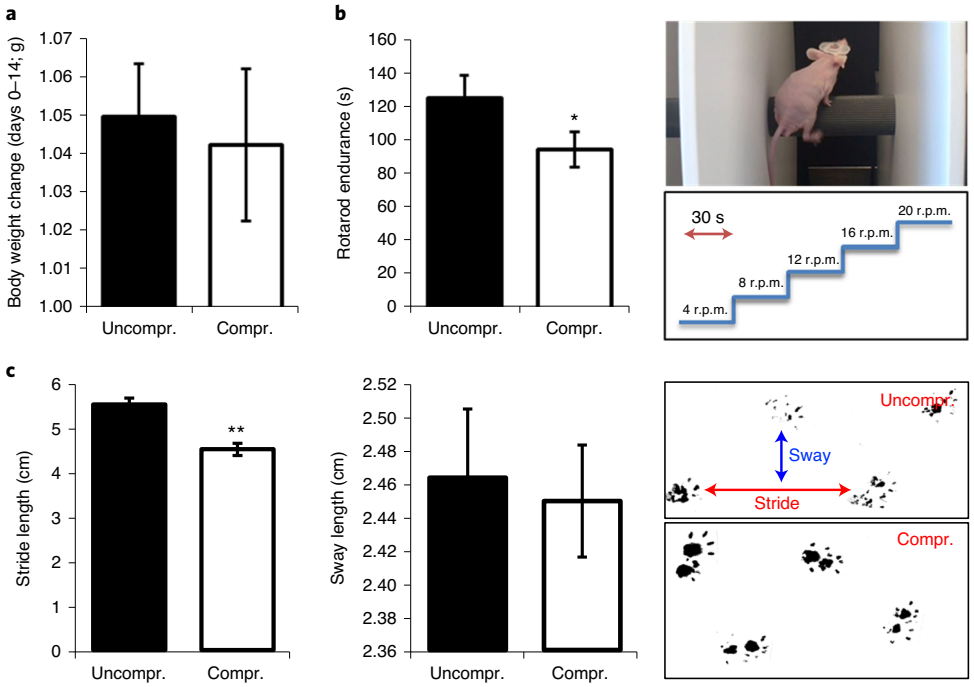

Fig. 9 | Chronic compression results in behavioral responses that can be quantified via different functional tests. a, **b**, Although mouse body weight did not show a substantial reduction (**a**), endurance in the Rotarod test substantially decreased after chronic compression (**b**). **c**, The alteration in motor coordination was also reflected in stride length and sway length, additional functional assays that test the effects of chronic compression on brain. $^{*}P < .05$; $^{**}P < .01$, Student's two-tailed unpaired t test; $n = 4$. Animal procedures in this work were carried out according to the Public Health Service Policy on Humane Care of Laboratory Animals and approved by the Institutional Animal Care and Use Committee of Massachusetts General Hospital. Parts of this figure are adapted from ref. [14], Springer Nature.

Reporting Summary

Further information on research design is available in the Nature Research Reporting Summary linked to this article.

Data availability

The datasets generated and/or analyzed during the current study are available from the corresponding author upon request.

Code availability

The code associated with the datasets generated and/or analyzed during the current study is available from the corresponding author upon request.

References

1. Jain, R. K., Martin, J. D. & Stylianopoulos, T. The role of mechanical forces in tumor growth and therapy. *Annu. Rev. Biomed. Eng.* **16**, 321–346 (2014).
2. Mitchell, M. J., Jain, R. K. & Langer, R. Engineering and physical sciences in oncology: challenges and opportunities. *Nat. Rev. Cancer* **17**, 659–675 (2017).
3. Helmlinger, G. et al. Solid stress inhibits the growth of multicellular tumor spheroids. *Nat. Biotechnol.* **15**, 778–783 (1997).
4. Stylianopoulos, T. et al. Causes, consequences, and remedies for growth-induced solid stress in murine and human tumors. *Proc. Natl Acad. Sci. USA* **109**, 15101–15108 (2012).
5. Nia, H. T. et al. Solid stress and elastic energy as measures of tumour mechanopathology. *Nat. Biomed. Eng.* **1**, 0004 (2016).
6. Padera, T. P. et al. Pathology: cancer cells compress intratumour vessels. *Nature* **427**, 695 (2004).
7. Chauhan, V. P. et al. Angiotensin inhibition enhances drug delivery and potentiates chemotherapy by decompressing tumour blood vessels. *Nat. Commun.* **4**, 2516 (2013).
8. Chauhan, V. P. et al. Compression of pancreatic tumor blood vessels by hyaluronan is caused by solid stress and not interstitial fluid pressure. *Cancer Cell* **26**, 14–15 (2014).

9. Tse, J. M. et al. Mechanical compression drives cancer cells toward invasive phenotype. *Proc. Natl Acad. Sci. USA* **109**, 911–916 (2012).
10. Ricca, B. L. et al. Transient external force induces phenotypic reversion of malignant epithelial structures via nitric oxide signaling. *Elife* **7**, e26161 (2018).
11. Montel, F. et al. Stress clamp experiments on multicellular tumor spheroids. *Phys. Rev. Lett.* **107**, 188102 (2011).
12. Delarue, M. et al. Compressive stress inhibits proliferation in tumor spheroids through a volume limitation. *Biophys. J.* **107**, 1821–1828 (2014).
13. Fernández-Sánchez, M. E. et al. Mechanical induction of the tumorigenic β-catenin pathway by tumour growth pressure. *Nature* **523**, 92–95 (2015).
14. Seano, G. et al. Solid stress in brain tumours causes neuronal loss and neurological dysfunction and can be reversed by lithium. *Nat. Biomed. Eng.* **3**, 230–245 (2019).
15. Nia, H. T. et al. Quantifying solid stress and elastic energy from excised or in situ tumors. *Nat. Protoc.* **13**, 1091–1105 (2018).
16. Amidei, C. & Kushner, D. S. Clinical implications of motor deficits related to brain tumors. *Neurooncol. Prac.* **2**, 179–184 (2015).
17. Mukand, J. A. et al. Incidence of neurologic deficits and rehabilitation of patients with brain tumors. *Am. J. Phys. Med. Rehabil.* **80**, 346–350 (2001).
18. Kushner, D. S. & Amidei, C. Rehabilitation of motor dysfunction in primary brain tumor patients. *Neurooncol. Prac.* **2**, 185–191 (2015).
19. Sawaya, R. et al. Neurosurgical outcomes in a modern series of 400 craniotomies for treatment of parenchymal tumors. *Neurosurgery* **42**, 1044–1055 (1998). discussion 1055-1056.
20. Rees, J. H. Diagnosis and treatment in neuro-oncology: an oncological perspective. *Br. J. Radiol.* **84**(Spec. No. 2), S82–S89 (2011).
21. Farago, N. et al. Human neuronal changes in brain edema and increased intracranial pressure. *Acta Neuropathol. Commun.* **4**, 78 (2016).
22. Goriely, A. et al. Mechanics of the brain: perspectives, challenges, and opportunities. *Biomech. Model. Mechanobiol.* **14**, 931–965 (2015).
23. Unterberg, A. W. et al. Edema and brain trauma. *Neuroscience* **129**, 1021–1029 (2004).
24. de Groot, J. & Sontheimer, H. Glutamate and the biology of gliomas. *Glia* **59**, 1181–1189 (2011).
25. Sontheimer, H. A role for glutamate in growth and invasion of primary brain tumors. *J. Neurochem.* **105**, 287–295 (2008).
26. Savaskan, N. E. et al. Neurodegeneration in the brain tumor microenvironment: glutamate in the limelight. *Curr. Neuropharmacol.* **13**, 258–265 (2015).
27. Huisman, T. A. Tumor-like lesions of the brain. *Cancer Imaging* **9**(Special Issue A), S10–S13 (2009).
28. Cunliffe, C. H. et al. Intracranial lesions mimicking neoplasms. *Arch. Pathol. Lab. Med.* **133**, 101–123 (2009).
29. Askoxylakis, V. et al. A cerebellar window for intravital imaging of normal and disease states in mice. *Nat. Protoc.* **12**, 2251–2262 (2017).
30. Snuderl, M. et al. Targeting placental growth factor/neuropilin 1 pathway inhibits growth and spread of medulloblastoma. *Cell* **152**, 1065–1076 (2013).
31. Bar-Kochba, E. et al. Strain and rate-dependent neuronal injury in a 3D in vitro compression model of traumatic brain injury. *Sci. Rep.* **6**, 30550 (2016).
32. Lusardi, T. A. et al. Effect of acute calcium influx after mechanical stretch injury in vitro on the viability of hippocampal neurons. *J. Neurotrauma* **21**, 61–72 (2004).
33. Pfister, B. J. et al. An in vitro uniaxial stretch model for axonal injury. *Ann. Biomed. Eng.* **31**, 589–598 (2003).
34. Teixeira, F. G. et al. Bioengineered cell culture systems of central nervous system injury and disease. *Drug Discov. Today* **21**, 1456–1463 (2016).
35. Schoeler, M. et al. Dexmedetomidine is neuroprotective in an in vitro model for traumatic brain injury. *BMC Neurol.* **12**, 20 (2012).
36. Morrison, B. III et al. An in vitro model of traumatic brain injury utilising two-dimensional stretch of organotypic hippocampal slice cultures. *J. Neurosci. Methods* **150**, 192–201 (2006).
37. Xu, B. N. et al. Pathophysiology of brain swelling after acute experimental brain compression and decompression. *Neurosurgery* **32**, 289–296 (1993). discussion 296.
38. Miller, J. D., Stanek, A. E. & Langfitt, T. W. Cerebral blood flow regulation during experimental brain compression. *J. Neurosurg.* **39**, 186–196 (1973).
39. Leech, P. & Miller, J. D. Intracranial volume–pressure relationships during experimental brain compression in primates: 1. Pressure responses to changes in ventricular volume. *J. Neurol. Neurosurg. Psychiatry* **37**, 1093–1098 (1974).
40. De la Torre, J. C. et al. Dimethyl sulfoxide in the treatment of experimental brain compression. *J. Neurosurg.* **38**, 345–354 (1973).
41. Sullivan, H. G. et al. The physiological basis of intracranial pressure change with progressive epidural brain compression. An experimental evaluation in cats. *J. Neurosurg.* **47**, 532–550 (1977).
42. Schettini, A. & Walsh, E. K. Brain tissue elastic behavior and experimental brain compression. *Am. J. Physiol.* **255**(5 Pt 2), R799–R805 (1988).
43. Schettini, A. & Walsh, E. K. Brain elastic behavior in experimental brain compression: influence of steroid therapy. *Brain Res.* **305**, 141–143 (1984).

44. Calabrese, E. et al. A diffusion MRI tractography connectome of the mouse brain and comparison with neuronal tracer data. *Cereb. Cortex* **25**, 4628–4637 (2015).
45. Kober, F., Duhamel, G. & Callot, V. Cerebral perfusion MRI in mice, in In Vivo NMR Imaging 117-138 (Springer, New York, 2011).
46. Kearney, S. P. et al. Simultaneous 3D MR elastography of the in vivo mouse brain. *Phys. Med. Biol.* **62**, 7682–7693 (2017).
47. Kamoun, W. S. et al. Simultaneous measurement of RBC velocity, flux, hematocrit and shear rate in vascular networks. *Nat. Methods* **7**, 655–660 (2010).
48. Fukumura, D. et al. Tumor microvasculature and microenvironment: novel insights through intravital imaging in pre-clinical models. *Microcirculation* **17**, 206–225 (2010).
49. Jain, R. K., Munn, L. L. & Fukumura, D. Dissecting tumour pathophysiology using intravital microscopy. *Nat. Rev. Cancer* **2**, 266–276 (2002).
50. Blatter, C. et al. Simultaneous measurements of lymphatic vessel contraction, flow and valve dynamics in multiple lymphangions using optical coherence tomography. *J. Biophotonics Vol.* **11**, e201700017 (2018).
51. Blatter, C. et al. In vivo label-free measurement of lymph flow velocity and volumetric flow rates using Doppler optical coherence tomography. *Sci. Rep.* **6**, 29035 (2016).
52. Vakoc, B. J. et al. Three-dimensional microscopy of the tumor microenvironment in vivo using optical frequency domain imaging. *Nat. Med.* **15**, 1219–1223 (2009).
53. Kamoun, W. S. et al. Edema control by cediranib, a vascular endothelial growth factor receptor–targeted kinase inhibitor, prolongs survival despite persistent brain tumor growth in mice. *J. Clin. Oncol.* **27**, 2542–2552 (2009).
54. Boucher, Y. et al. Interstitial fluid pressure in intracranial tumours in patients and in rodents. *Br. J. Cancer* **75**, 829–836 (1997).
55. Brooks, S. P., Trueman, R. C. & Dunnett, S. B. Assessment of motor coordination and balance in mice using the Rotarod, elevated bridge, and footprint tests. *Curr. Protoc. Mouse Biol.* **2**, 37–53 (2012).
56. Arvanitis, C. D. et al. Mechanisms of enhanced drug delivery in brain metastases with focused ultrasound-induced blood–tumor barrier disruption. *Proc. Natl Acad. Sci. USA* **115**, e8717–e8726 (2018).
57. Dong, H. W. *The Allen Reference Atlas: A Digital Color Brain Atlas of the C57Bl/6J Male Mouse* ix, 366 (Wiley, 2008).

Acknowledgements

This work was supported in part by the National Cancer Institute (P01-CA080124, R35-CA197743, U01-CA224173, and R01-CA208205 to R.K.J.; F32-CA216944 to H.T.N), the American Association of Cancer Research (19-40-50-DATT to M.D.), the Susan G. Komen Foundation (PDF14201739 to G.S.), and the European Research Council (ERC; 805225 to G.S.). R.K.J.'s research is also supported by grants from the National Foundation for Cancer Research, Harvard Ludwig Center, Jane's Trust Foundation, and the Bill and Melinda Gates Foundation.

Author contributions

H.T.N., M.D., G.S., W.W.H., S.R., P.H., L.L.M., and R.K.J. designed the study; H.T.N., M.D., G.S., S.R., and P.H. acquired the data. H.T.N., M.D., G.S., and R.K.J. contributed to analysis and interpretation of the data. H.T.N., M.D., G.S., S.Z., W.W.H., S.R., P.H., L.L.M., and R.K.J. were involved in drafting the article and revising it for important intellectual content.

Competing interests

R.K.J. received an honorarium from Amgen; consultant fees from Chugai, Enlight, Merck, Ophthotech, Pfizer, SPARC, SynDevRx, and XTuit; owns equity in Enlight, Ophthotech, and SynDevRx; and serves on the boards of trustees of Tekla Healthcare Investors, Tekla Life Sciences Investors, Tekla Healthcare Opportunities Fund, and Tekla World Healthcare Fund. No funding or reagents from these companies were used in this study.

Additional information

Supplementary information is available for this paper at https://doi.org/10.1038/s41596-020-0328-2.

Correspondence and requests for materials should be addressed to R.K.J.

Reprints and permissions information is available at www.nature.com/reprints.

Publisher's note Springer Nature remains neutral with regard to jurisdictional claims in published maps and institutional affiliations.

Received: 8 December 2018; Accepted: 6 April 2020;
Published online: 17 July 2020

Related links
Key reference using this protocol
Seano, G. et al. *Nat. Biomed. Eng.* **3**, 230–245 (2019): https://doi.org/10.1038/s41551-018-0334-7

nature research

Corresponding author(s): Rakesh K. Jain

Last updated by author(s): Sep 24, 2019

Reporting Summary

Nature Research wishes to improve the reproducibility of the work that we publish. This form provides structure for consistency and transparency in reporting. For further information on Nature Research policies, see Authors & Referees and the Editorial Policy Checklist.

Statistics

For all statistical analyses, confirm that the following items are present in the figure legend, table legend, main text, or Methods section.

n/a	Confirmed	
☐	☒	The exact sample size (*n*) for each experimental group/condition, given as a discrete number and unit of measurement
☐	☒	A statement on whether measurements were taken from distinct samples or whether the same sample was measured repeatedly
☐	☒	The statistical test(s) used AND whether they are one- or two-sided *Only common tests should be described solely by name; describe more complex techniques in the Methods section.*
☒	☐	A description of all covariates tested
☒	☐	A description of any assumptions or corrections, such as tests of normality and adjustment for multiple comparisons
☒	☐	A full description of the statistical parameters including central tendency (e.g. means) or other basic estimates (e.g. regression coefficient) AND variation (e.g. standard deviation) or associated estimates of uncertainty (e.g. confidence intervals)
☐	☒	For null hypothesis testing, the test statistic (e.g. *F*, *t*, *r*) with confidence intervals, effect sizes, degrees of freedom and *P* value noted *Give P values as exact values whenever suitable.*
☒	☐	For Bayesian analysis, information on the choice of priors and Markov chain Monte Carlo settings
☒	☐	For hierarchical and complex designs, identification of the appropriate level for tests and full reporting of outcomes
☒	☐	Estimates of effect sizes (e.g. Cohen's *d*, Pearson's *r*), indicating how they were calculated

Our web collection on statistics for biologists contains articles on many of the points above.

Software and code

Policy information about availability of computer code

Data collection	*Provide a description of all commercial, open source and custom code used to collect the data in this study, specifying the version used OR state that no software was used.*
Data analysis	The following commercial software were used to analyze the results: VisualSonics software, SolidWorks, ABAQUS Version 6.9, Bitplane Imaris 7.0 Image Analysis software, Graphpad Prism 7, Microsoft Excel. Moreover, we used previously published MATLAB and ImageJ custom algorithms.

For manuscripts utilizing custom algorithms or software that are central to the research but not yet described in published literature, software must be made available to editors/reviewers. We strongly encourage code deposition in a community repository (e.g. GitHub). See the Nature Research guidelines for submitting code & software for further information.

Data

Policy information about availability of data

All manuscripts must include a data availability statement. This statement should provide the following information, where applicable:

- Accession codes, unique identifiers, or web links for publicly available datasets
- A list of figures that have associated raw data
- A description of any restrictions on data availability

The datasets generated and/or analyzed during the current study and associated codes are available from the corresponding author upon request.

Field-specific reporting

Please select the one below that is the best fit for your research. If you are not sure, read the appropriate sections before making your selection.

☒ Life sciences ☐ Behavioural & social sciences ☐ Ecological, evolutionary & environmental sciences

For a reference copy of the document with all sections, see nature.com/documents/nr-reporting-summary-flat.pdf

Life sciences study design

All studies must disclose on these points even when the disclosure is negative.

Sample size	No sample-size calculation was performed because all animal studies were built with the maximum technically feasible number of animals. Since the surgical complexities in cranial window and compression device implantation, this number were not able to be more than 6-8 per experiment.
Data exclusions	No data were excluded from the presented analyses.
Replication	Each result presented is at least a duplicate of experiments or animal studies. All attempts at replication were successful.
Randomization	Mice were randomized by pre-treatment Rotarod endurance and body weight.
Blinding	Blinding during analysis was used for all the experiments.

Reporting for specific materials, systems and methods

We require information from authors about some types of materials, experimental systems and methods used in many studies. Here, indicate whether each material, system or method listed is relevant to your study. If you are not sure if a list item applies to your research, read the appropriate section before selecting a response.

Materials & experimental systems

n/a	Involved in the study
☐	☒ Antibodies
☐	☒ Eukaryotic cell lines
☒	☐ Palaeontology
☐	☒ Animals and other organisms
☒	☐ Human research participants
☒	☐ Clinical data

Methods

n/a	Involved in the study
☒	☐ ChIP-seq
☒	☐ Flow cytometry
☒	☐ MRI-based neuroimaging

Antibodies

Antibodies used	Mouse anti-NeuN (Chemicon, MAB377), rabbit anti-GFP (Cell Signaling Technology, #2956), rabbit anti-CC3 (Cell Signaling Technology, mAb #9664), rabbit anti-LC3-II (Cell Signaling Technology, #12741); Apoptag (ApopTag Peroxidase In Situ Apoptosis Detection Kit, #S7100, Millipore) was used as a marker for apoptosis.
Validation	Antibody validation principles from Cell Signaling Technology were employed, including the use of any and all appropriate negative and positive controls.

Eukaryotic cell lines

Policy information about cell lines

Cell line source(s)	ATCC
Authentication	All cell lines were authenticated before use by IDEXX Laboratories (IDEXX , Human 9 and 16 species-specific STR marker profile)
Mycoplasma contamination	All cell lines were repeatedly tested and were negative for mycoplasma using the Mycoalert Plus Mycoplasma Detection Kit (Lonza).
Commonly misidentified lines (See ICLAC register)	No commonly misidentified cell lines were used.

Animals and other organisms

Policy information about studies involving animals; ARRIVE guidelines recommended for reporting animal research

Laboratory animals	Female nude mice, ages 8-12 weeks
Wild animals	The study did not involve wide animals
Field-collected samples	The study did not involve samples collected in the field.
Ethics oversight	All animal protocols were approved by and in accordance with the guidelines established by the Institutional Animal Care and Use Committee (IACUC) at Massachusetts General Hospital (MGH). The mouse colony (MGH Cox7) was maintained in accordance with National Institutes of Health and MGH guidelines. MGH is accredited with the International Association for Assessment and Accreditation of Laboratory Animal Care (AAALAC) and the NIH Office of Laboratory Animal Welfare (A3596-01).

Note that full information on the approval of the study protocol must also be provided in the manuscript.